

# Nearest-Neighbor Radii under Dependent Sampling

Yuanyuan Gao<sup>1,\*</sup> Yilong Hou<sup>2,\*</sup> Zhexiao Lin<sup>1,\*,†</sup>

<sup>1</sup>Department of Statistics, University of California, Berkeley, CA 94720, USA

<sup>2</sup>Department of Biostatistics, University of California, Berkeley, CA 94720, USA

May 15, 2026

## Abstract

Nearest-neighbor methods are fundamental to classical and modern machine learning, yet their geometric properties are typically analyzed under independent sampling. In this paper, we study the nearest-neighbor radii under dependent sampling. We consider strong mixing dependent observations and ask whether dependence changes the scale of nearest-neighbor neighborhoods. We establish distribution-free almost sure convergence under polynomial mixing and sharp non-asymptotic moment bounds under geometric mixing. The moment bounds depend on the local intrinsic dimension rather than the ambient dimension, making the results applicable to high-dimensional data concentrated near lower-dimensional manifolds. Synthetic experiments and real-world time-series benchmarks support the theory, showing that nearest-neighbor geometry remains informative under dependence sampling.

## 1 Introduction

Nearest-neighbor (NN) methods remain one of the most fundamental ideas in machine learning. They underlie classical procedures such as  $k$ -nearest-neighbor classification (Cover and Hart, 1967) and regression (Stone, 1977), nonparametric density estimation and local averaging (Loftsgaarden and Quesenberry, 1965), and they also appear implicitly in a much broader range of modern techniques built on local neighborhoods, including graph-based semi-supervised learning (Zhu et al., 2003), manifold methods (Belkin and Niyogi, 2003), information retrieval (Wang et al., 2021), and language modeling (Khandelwal et al., 2021; Xu et al., 2023a,b). In all of these methods, a basic geometric quantity at the center of the analysis is the distance from a query point  $x$  to its  $k$ th nearest neighbor in the sample.

---

\*Authors are listed in alphabetical order.

†Corresponding author: zhexiaolin@berkeley.edu.

This random radius determines the scale of the local neighborhood around  $x$ , and therefore controls how much of the ambient space the method actually “sees.”

From a statistical perspective, nearest-neighbor radii determine the central bias–variance tradeoff of local methods (Stone, 1977; Biau and Devroye, 2015). If the radius is too large, a local estimator averages over points that are geometrically far from the query and thus introduces bias. If the radius is too small, the estimator uses too few effective observations and becomes unstable. In density estimation, the  $k$ -NN radius is the random bandwidth that determines the volume of the adaptive neighborhood. In regression and classification, it controls the locality of smoothing. In manifold and graph-based methods, it determines neighborhood connectivity and the scale at which local geometry is resolved. Understanding the scaling of the  $k$ -NN radius is therefore a prerequisite for understanding the performance of a wide class of machine learning algorithms.

In the classical i.i.d. setting, the behavior of  $k$ -NN radius is well understood: under standard local mass conditions, the canonical scale is  $(k/n)^{1/d}$ , or more generally,  $(k/n)^{1/s}$  when the local geometry is determined by an intrinsic dimension  $s$  (Loftsgaarden and Quesenberry, 1965; Biau and Devroye, 2015; Kpotufe, 2011). However, many learning problems do not arise from independent samples. Data are often collected sequentially, spatially, or through interaction with a dynamical environment. Examples include time-series forecasting, reinforcement learning from trajectories, sequential recommendation, event streams, dependent tabular logs, and spatiotemporal sensing (Mohri and Rostamizadeh, 2010; Tu et al., 2024). In such settings, observations can be strongly dependent even when their marginal distribution is stable. This raises a basic question:

*How does dependence affect the geometry of nearest-neighbor neighborhoods?*

This question is both mathematically natural and practically important. A large body of machine learning theory relies on i.i.d. nearest-neighbor geometry either explicitly or implicitly. Yet once dependence is present, standard concentration arguments no longer apply directly, and even basic geometric quantities such as the  $k$ -NN radius become more delicate. If dependence were to fundamentally change the scaling of nearest-neighbor radii, then the geometry underlying many local learning procedures would also change. On the other hand, if the canonical radius scale remains unchanged under weak dependence, this would help justify the use of nearest-neighbor and local methods beyond the i.i.d. regime.

In this paper, we study the nearest-neighbor radii under dependent sampling. We consider a triangular array of  $\mathbb{R}^d$ -valued observations with a common marginal distribution and strong mixing dependence along each row. This framework is general enough to cover the usual stationary-sequence setting as a special case, while also allowing the dependence structure to vary with  $n$ . Our object of study is the radius  $R_{n,k}(x) := \|\mathcal{X}_{(k)}^n(x) - x\|$ , that is, the distance from a fixed query point  $x$  to its  $k$ th nearest neighbor among the  $n$  observations in the row.

Our first result is almost sure convergence: under polynomial  $\alpha$ -mixing, we show that the nearest-neighbor radius converges almost surely to the distance from  $x$  to the support of the marginal law. This gives a dependent-sampling analogue of the classical consistency result and shows that weak dependence does not change the limiting geometry of nearest-neighbor radii. We then develop a non-asymptotic theory under geometric mixing. Under a local lower-mass condition of order  $s$ , we establish a tail bound for  $R_{n,k}(x)$  and derive the sharp moment upper bound  $\mathbb{E}[R_{n,k}(x)^p] \lesssim (k/n)^{p/s}$  in the standard regime  $k \gtrsim \log n$ . Under a matching local upper-mass condition of order  $s$ , we also establish the matching lower bound and hence obtain the exact order  $\mathbb{E}[R_{n,k}(x)^p] \asymp (k/n)^{p/s}$ . Thus, geometric dependence changes the concentration mechanism, but not the fundamental exponent.

A key feature of our theory is that it is formulated in terms of a local exponent  $s > 0$ , rather than the ambient dimension  $d$ . This point is especially relevant for modern machine learning, where high-dimensional data often concentrate near lower-dimensional latent structures (Fefferman et al., 2016; Ansuini et al., 2019). Our results therefore support the common regime in which the effective geometry around the query point is lower-dimensional than the ambient space. In this sense, our results are not only about dependence, but also about how dependence interacts with local geometric complexity.

**Our contributions.** The main contributions are as follows.

1. We establish a *distribution-free almost sure convergence theorem* for the  $k$ -NN radius under polynomial  $\alpha$ -mixing. This extends the classical i.i.d. consistency result to dependent triangular arrays.
2. Under geometric  $\alpha$ -mixing and a local lower-mass condition of order  $s$ , we establish a *non-asymptotic tail bound* for the  $k$ -NN radius and derive the *sharp moment upper bound*  $\mathbb{E}[R_{n,k}(x)^p] \lesssim (k/n)^{p/s}$  for all  $p > 0$  in the standard dependent regime  $k \gtrsim \log n$ .
3. Under a matching local upper-mass condition, we establish a *matching lower bound*  $\mathbb{E}[R_{n,k}(x)^p] \gtrsim (k/n)^{p/s}$ , and hence obtain the *exact-order characterization*  $\mathbb{E}[R_{n,k}(x)^p] \asymp (k/n)^{p/s}$ .
4. Our theory is stated in terms of a *local geometric exponent*  $s$ , which yields an intrinsic-dimension interpretation and is relevant for modern high-dimensional learning problems.

We believe the main message is simple and useful: under weak dependence, nearest-neighbor geometry remains essentially the same as in the independent case at the level of its canonical scale. This provides theoretical support for transferring geometric intuition and local-method design principles from the i.i.d. world to substantially broader dependent settings.

## 1.1 Related work

**Applications of nearest-neighbor methods.** In recent years, nearest-neighbor methods have re-emerged in modern machine learning as a flexible mechanism for retrieval, adaptation, and locality in learned representation spaces. Examples include self-supervised representation learning (Avdiukhin et al., 2024; Long et al., 2025), tabular deep learning (Gorishniy et al., 2023), vector search and approximate nearest-neighbor infrastructure (Chen et al., 2021; Yang et al., 2024; Jääsaari et al., 2024; Wang et al., 2021), and robust retrieval and vision (Wu et al., 2022; Nizan and Tal, 2024). Beyond core machine learning, nearest-neighbor structure also plays an important role in causal inference through matching estimators (Abadie and Imbens, 2006, 2011; Lin et al., 2023; Lin and Han, 2025; Cattaneo et al., 2025), in rank-based and graph-based measures of dependence (Chatterjee, 2021; Azadkia and Chatterjee, 2021; Han, 2021; Lin and Han, 2022, 2023, 2024; Shi et al., 2024; Han and Huang, 2024), in information-theoretic functional estimation via  $k$ -NN entropy and mutual-information estimators (Kozachenko and Leonenko, 1987; Kraskov et al., 2004), and in multivariate nonparametric testing based on geometric graphs (Friedman and Rafsky, 1979; Henze and Penrose, 1999). This breadth of applications makes the geometric behavior of nearest-neighbor neighborhoods a foundational issue.

**Theory of nearest-neighbor methods under dependence.** Despite the wide range of applications, previous literature on the theory under dependence has mostly analyzed estimators built from nearest-neighbor neighborhoods, rather than the geometry of the neighborhoods themselves. Examples include nearest-neighbor classification with dependent training sequences (Holst and Irle, 2001) and rates for nearest-neighbor estimation under more general non-i.i.d. sampling schemes (Kulkarni and Posner, 1995). More broadly, the literature on learning from dependent observations has developed both positive and negative results for nonparametric prediction under mixing, ergodic, and other non-i.i.d. assumptions (Yu, 1994; Nobel, 1999; Mohri and Rostamizadeh, 2010). By contrast, our focus is on the radius itself as a primary object. This shift in perspective is useful because the nearest-neighbor radius serves as the random local scale in many downstream methods, so controlling it directly provides a geometric ingredient for analyzing local learning methods.

## 2 Setup

We study the geometry of nearest neighbors under dependent sampling. Let  $[X_{n,i} : 1 \leq i \leq n, n \geq 1]$  be a triangular array of  $\mathbb{R}^d$ -valued random variables defined on a common probability space  $(\Omega, \mathcal{F}, \mathbb{P})$ , where the ambient dimension  $d \geq 1$  is fixed. For each row  $n$ , the observations  $X_{n,1}, \dots, X_{n,n}$  could be independent, but we assume that they share a common marginal law  $\mu$  on  $\mathbb{R}^d$ . Thus, for every  $n \geq 1$  and every  $i \in \{1, \dots, n\}$ ,  $X_{n,i} \sim \mu$ .

This formulation distinguishes two roles in our analysis. The common marginal distribution  $\mu$  determines the local geometry of the marginal distribution, while the dependence structure controls how much effective information is contained in a sample of size  $n$ . Allowing the dependence structure to vary with  $n$  leads naturally to a triangular-array framework, which is flexible enough to cover the usual stationary-sequence setting as a special case and at the same time convenient for stating non-asymptotic results uniformly in  $n$ .

**Triangular-array strong mixing.** For integers  $1 \leq k \leq m \leq n$ , let  ${}^n\mathcal{F}_k^m := \sigma(X_{n,i} : k \leq i \leq m)$  denote the  $\sigma$ -field generated by the segment  $(X_{n,k}, \dots, X_{n,m})$  in the  $n$ th row. Following the standard strong-mixing framework, define the mixing coefficients of the triangular array by

$$\alpha_m := \sup_{n \geq 1} \sup_{1 \leq k \leq n-m} \sup \left\{ |\mathbb{P}(A \cap B) - \mathbb{P}(A)\mathbb{P}(B)| : A \in {}^n\mathcal{F}_1^k, B \in {}^n\mathcal{F}_{k+m}^n \right\}, \quad m \geq 1.$$

The array is said to be *strong mixing* (or  $\alpha$ -*mixing*) if

$$\alpha_m \rightarrow 0 \quad \text{as } m \rightarrow \infty.$$

The strong-mixing framework is classical in probability and time-series analysis (Bradley, 2005). This definition requires a uniform decay of dependence across all rows of the array. Intuitively, if two collections of variables are separated by at least  $m$  indices within the same row, then their dependence becomes weak when  $m$  is large. This is the dependence notion used throughout the paper.

The triangular-array formulation is more general than working with a single stationary process  $[X_i]_{i \geq 1}$ . It allows the dependence structure to vary with  $n$ , while keeping the marginal distribution fixed. We state finite-sample results uniformly in  $n$ , which also covers the usual time-series setting as a special case by taking  $X_{n,i} = X_i$  for  $1 \leq i \leq n$ . Therefore, readers who prefer the standard sequential viewpoint may regard our framework as a generalization.

**Nearest-neighbor radii.** Fix a query point  $x \in \mathbb{R}^d$ . For each  $n \geq 1$  and  $k \in \{1, \dots, n\}$ , let

$$\mathcal{X}_{(k)}^n(x) \in \{X_{n,1}, \dots, X_{n,n}\}$$

denote the  $k$ th nearest neighbor of  $x$  among the sample points in the  $n$ th row, with ties broken arbitrarily. We introduce the  $k$ -NN radius:

$$R_{n,k}(x) := \|\mathcal{X}_{(k)}^n(x) - x\|,$$

together with the local counting process:

$$N_n(x, r) := \sum_{i=1}^n \mathbf{1}\{\|X_{n,i} - x\| \leq r\}.$$

These two quantities are equivalent through the relationship

$$R_{n,k}(x) > r \iff N_n(x, r) < k.$$

This observation is the starting point for our entire analysis: upper bounds on the radius are equivalent to lower bounds for the number of sample points falling in  $B(x, r)$ . Under independence,  $N_n(x, r)$  is binomial with parameters  $n$  and  $\mu(B(x, r))$ , so its behavior can be analyzed using classical binomial tail bounds. Under dependence, however, this analysis is not applicable since the indicators  $\mathbf{1}\{\|X_{n,i} - x\| \leq r\}$  are dependent, and hence the local counting process is not binomial. Controlling  $R_{n,k}(x)$  therefore requires concentration arguments for dependent sequences, which is one of the main technical challenges.

**Support and target limit.** The asymptotic behavior of  $R_{n,k}(x)$  depends on the position of the query point relative to the support of  $\mu$ . Define

$$\text{supp}(\mu) := \{x \in \mathbb{R}^d : \mu(B(x, r)) > 0 \text{ for all } r > 0\},$$

where  $B(x, r)$  denotes the closed Euclidean ball centered at  $x$  with radius  $r$ . We also define the distance from  $x$  to the support of  $\mu$  by

$$r_x := \inf_{y \in \text{supp}(\mu)} \|y - x\|.$$

When  $x \in \text{supp}(\mu)$ , one has  $r_x = 0$ ; otherwise  $r_x$  is the deterministic limit that the  $k$ -NN radius converges to under mild assumptions.

### 3 Main results

We now present the main results for the  $k$ -NN radius under dependent sampling. As discussed in Section 2, the behavior of  $R_{n,k}(x) = \|\mathcal{X}_{(k)}^n(x) - x\|$  depends on both the dependence structure of the sample and the local geometry of the marginal law around the query point  $x$ . The almost sure limit is determined by the position of  $x$  relative to the support of  $\mu$ , whereas the convergence rate depends on how the mass of  $\mu$  accumulates near  $x$ .

#### 3.1 Distribution-free almost sure convergence

Our first theorem shows that the almost sure convergence of the  $k$ -NN radius to  $r_x$  holds under weak dependence.

**Theorem 1.** *Assume that the triangular array  $[X_{n,i}]_{1 \leq i \leq n, n \geq 1}$  is  $\alpha$ -mixing with coefficients  $[\alpha_m]_{m \geq 1}$  satisfying  $\alpha_m \lesssim m^{-\gamma}$  for some  $\gamma > 1$ . If  $k/n \rightarrow 0$ , then*

$$\|\mathcal{X}_{(k)}^n(x) - x\| \xrightarrow{\text{a.s.}} r_x.$$

In particular, if  $x \in \text{supp}(\mu)$  and  $k/n \rightarrow 0$ , then

$$\|\mathcal{X}_{(k)}^n(x) - x\| \xrightarrow{\text{a.s.}} 0.$$

Theorem 1 may be viewed as the dependent-sampling analogue of the classical i.i.d. consistency result (Biau and Devroye, 2015, Lemma 2.2). It shows that weak dependence, quantified here through a polynomial mixing condition, does not change the limiting geometric behavior of nearest-neighbor radii. Importantly, the result remains distribution-free: no density, smoothness, or local mass condition is required. The only assumption is that dependence decays polynomially fast along each row of the triangular array.

### 3.2 From almost sure convergence to moment bounds

We next turn to non-asymptotic moment results. For these stronger results, one must quantify how much probability mass lies near the query point  $x$ .

Rather than working with the ambient dimension  $d$ , we state the results using a general local exponent  $s > 0$ . This formulation is more flexible and captures the possibility that the effective local dimension near  $x$  is smaller than the ambient dimension. The standard Euclidean case is recovered by setting  $s = d$ .

For the non-asymptotic results, we impose the stronger assumption that the mixing coefficients decay exponentially fast.

**Assumption 1** (Geometric  $\alpha$ -mixing). *There exists  $\gamma > 0$  such that  $\alpha_m \leq e^{-\gamma m}$  for all  $m \geq 1$ .*

Assumption 1 strengthens the assumption in Theorem 1 from polynomial to exponential decorrelation. This stronger assumption enables non-asymptotic concentration via blocking arguments. The parameter  $\gamma$  quantifies the strength of dependence: larger  $\gamma$  corresponds to faster decorrelation, and in the limit of vanishing dependence, one recovers behavior close to the i.i.d. case.

Geometric mixing is a standard assumption in time-series theory and is satisfied by many classical models under mild regularity conditions (Doukhan, 2012). In particular, stationary ARMA processes are known to be strongly mixing with exponential rate under standard stability assumptions (Mokkadem, 1988), which makes geometric mixing a natural benchmark for studying dependent nearest-neighbor geometry.

**Assumption 2** (Local lower mass of order  $s$  at  $x$ ). *There exist constants  $c_- > 0$ ,  $r_0 > 0$ , and  $s > 0$  such that  $\mu(B(x, r)) \geq c_- r^s$  for all  $0 < r \leq r_0$ .*

Assumption 2 guarantees that the ball  $B(x, r)$  contains enough probability mass for its radius- $r$  neighborhood to capture roughly  $nr^s$  sample points. This lower bound is the key ingredient for the upper bound of  $R_{n,k}(x)$ .

**Assumption 3** (Local upper mass of order  $s$  at  $x$ ). *There exist constants  $c_+ > 0$ ,  $r_0 > 0$ , and  $s > 0$  such that  $\mu(B(x, r)) \leq c_+ r^s$  for all  $0 < r \leq r_0$ .*

Assumption 3 matches Assumption 2 and prevents the distribution from placing too much mass near  $x$ , and is needed to establish a matching lower bound on the radius.

**Assumption 4** (Compact support). *The support of  $\mu$  is contained in a compact set of diameter at most  $D$ .*

Assumption 4 is for technical simplicity rather than a geometric limitation. The local behavior of the  $k$ -NN radius is determined by Assumptions 2 and 3, which quantify how the mass of  $\mu$  accumulates near the query point  $x$ . By contrast, compact support is used to control the far tail of  $R_{n,k}(x)$  when converting non-asymptotic tail bounds into moment bounds. Compact support ensures that the radius is uniformly bounded, which keeps the moment argument simpler. One could replace the compact support by a tail or moment condition on  $\mu$  at the cost of a more technical proof.

**Interpretation of the local exponent  $s$ .** The exponent  $s$  is the *local geometric dimension* around the query point  $x$ . Assumptions 2 and 3 say that, for sufficiently small radii,  $\mu(B(x, r)) \asymp r^s$ . Thus, the amount of probability mass captured by a small neighborhood of  $x$  grows like the volume of an  $s$ -dimensional ball. In the standard Euclidean case with a positive density in  $\mathbb{R}^d$ , one has  $s = d$ . More generally,  $s$  may be strictly smaller than  $d$ , e.g., when the distribution is concentrated near a lower-dimensional manifold, subspace, or other latent geometric structure. Our theory is therefore local and intrinsic: the scaling of the  $k$ -NN radius is determined by the intrinsic dimension of the distribution near  $x$ , rather than by the ambient Euclidean dimension.

Throughout the sharp upper-bound results, we work in the regime  $K_0 \log n \leq k \leq \kappa n$ , for some fixed  $K_0 > 0$  and  $0 < \kappa < c_- r_0^s / 8$ . The upper bound ensures that the radius remains within the local regime  $r \leq r_0$ , where Assumption 2 applies. The lower bound  $k \gtrsim \log n$  is due to dependence: it arises because the proof decouples the sample into blocks of length  $\asymp \log n$ , as is standard in Bernstein-type concentration arguments for geometric mixing sequences (Liebscher, 1996; Merlevède et al., 2009). In contrast, the lower bound on the radius does not require  $k \gtrsim \log n$ .

**On the regime  $k \gtrsim \log n$ .** The lower bound  $k \gtrsim \log n$  is the natural regime in which our blocking-based concentration argument resolves the dependence structure. It reflects the cost of decoupling geometric mixing observations into approximately independent blocks, rather than a change in the underlying nearest-neighbor geometry. In particular, our results suggest that dependence affects concentration through a logarithmic penalty, while the canonical radius scale remains  $(k/n)^{1/s}$ .

### 3.3 Non-asymptotic upper bound

We first establish a tail bound on  $R_{n,k}(x)$ .

**Theorem 2** (Non-asymptotic tail bound). *Assume Assumptions 1, 2, and 4. Define*

$$b_n := \left\lceil \frac{8}{\gamma} \log n \right\rceil, \quad r_*(n, k) := \left( \frac{8k}{c-n} \right)^{1/s}.$$

*Then there exists a constant  $c_0 > 0$ , depending only on  $\gamma$ , such that for every integer  $j \geq 0$  satisfying  $2^j r_*(n, k) \leq r_0$ , we have*

$$\mathbb{P}(R_{n,k}(x) > 2^j r_*(n, k)) \leq 4 \exp\left(-c_0 2^{js} \frac{k}{\log n}\right) + Cn^{-7},$$

*for all sufficiently large  $n$ .*

Theorem 2 shows that the  $k$ -NN radius is concentrated around the canonical geometric scale  $(k/n)^{1/s}$ . In particular, Theorem 2 separates the roles of geometry and dependence: the exponent  $1/s$  is determined by the local mass behavior of  $\mu$  near  $x$ , while the dependence structure enters only through the additional  $\log n$  factor in the concentration exponent, which is the price of the blocking argument under geometric mixing. Thus, although dependence weakens concentration relative to the i.i.d. case, it does not change the underlying nearest-neighbor scale. Theorem 2 implies a high-probability upper bound:

$$R_{n,k}(x) \lesssim \left( \frac{k + t \log n}{n} \right)^{1/s}$$

with probability at least  $1 - e^{-ct}$ , for some constant  $c > 0$ .

Integrating the tail bound yields the sharp moment upper bound.

**Theorem 3** (Sharp moment upper bound). *Assume Assumptions 1, 2, and 4. Let  $p > 0$ . Then there exists a constant  $C_{p,s} > 0$  such that, whenever  $K_0 \log n \leq k \leq \kappa n$ , we have*

$$\mathbb{E}[R_{n,k}(x)^p] \leq C_{p,s} \left( \frac{k}{n} \right)^{p/s}.$$

If  $\mu$  admits a density, then by the Lebesgue differentiation theorem, Assumption 2 holds with  $s = d$  for  $\mu$ -almost every interior point at which the density is positive. Consequently, Theorem 3 applies for  $\mu$ -almost all such  $x$ . Theorem 3 is applicable in downstream analyses, since many local learning bounds depend on moments of the random neighborhood. We discuss this further in the discussion section.

### 3.4 Matching non-asymptotic lower bound

To show that the exponent  $p/s$  is optimal, we next establish a matching lower bound. Unlike the upper bound, the lower bound is purely local and does not require any dependence condition.

**Theorem 4** (Matching lower bound). *Assume Assumption 3. Let  $p > 0$ . Then whenever  $(\frac{k}{2c_+n})^{1/s} \leq r_0$ , we have*

$$\mathbb{E}[R_{n,k}(x)^p] \geq \frac{1}{2} \left( \frac{k}{2c_+n} \right)^{p/s}.$$

Theorem 4 is conceptually simple but important: if a ball of radius  $r$  contains at most order  $r^s$  probability mass, then one cannot expect the  $k$ th nearest neighbor to lie much closer than  $(k/n)^{1/s}$ . Combining the upper and lower bounds yields the following exact-order characterization.

**Theorem 5** (Exact-order characterization). *Assume Assumptions 1, 2, 3, and 4, with the same exponent  $s > 0$ . Then for every  $p > 0$  there exist constants  $0 < c_{p,s} \leq C_{p,s} < \infty$  such that, for all sufficiently large  $n$  and all  $K_0 \log n \leq k \leq \kappa n$ , we have*

$$c_{p,s} \left( \frac{k}{n} \right)^{p/s} \leq \mathbb{E}[R_{n,k}(x)^p] \leq C_{p,s} \left( \frac{k}{n} \right)^{p/s}.$$

Theorem 5 shows that the canonical nearest-neighbor radii scale remains unchanged under geometric mixing. The dependence changes constants and concentration behavior, but not the fundamental exponent.

## 4 Experiments

### 4.1 Moment convergence rate

We test whether the moment-rate upper bound suggested by the proved  $\alpha$ -mixing setting remains visible under broader dependence structures. The implementation compares the i.i.d. benchmark with three dependent sequence models: a linear Gaussian state-space model, a hidden Markov model, and a stationary Gaussian-process sequence with a radial basis function (RBF)-like kernel generated by fast Fourier transform (FFT). All observations are marginally transformed to the cube  $[0, 1]^d$ .

We sample 1000 points uniformly from the interior of the cube and report the mean  $p$ -th moment of the  $k$ -NN radius. For each  $d \in \{1, 3, 5\}$ , we choose  $p$  such that  $p/d \in \{1, 2, 3, 4, 5\}$ . We use exponentially growing, dimension-dependent sample sizes  $n(d) = 100 \cdot 2^d \cdot m$  for  $m \in \{1, 2, 4, 8, 16, 32\}$ . The number of NNs is chosen as  $k = \lfloor n^\beta \rfloor$  with  $\beta$  on a 20-point grid in  $[0.1, 0.9]$  for slope fitting. The slope is the coefficient  $b$  from  $\log M = a + b \log(k/n)$ , with theoretical slope  $p/d$  for the i.i.d. and  $\alpha$ -mixing setting.

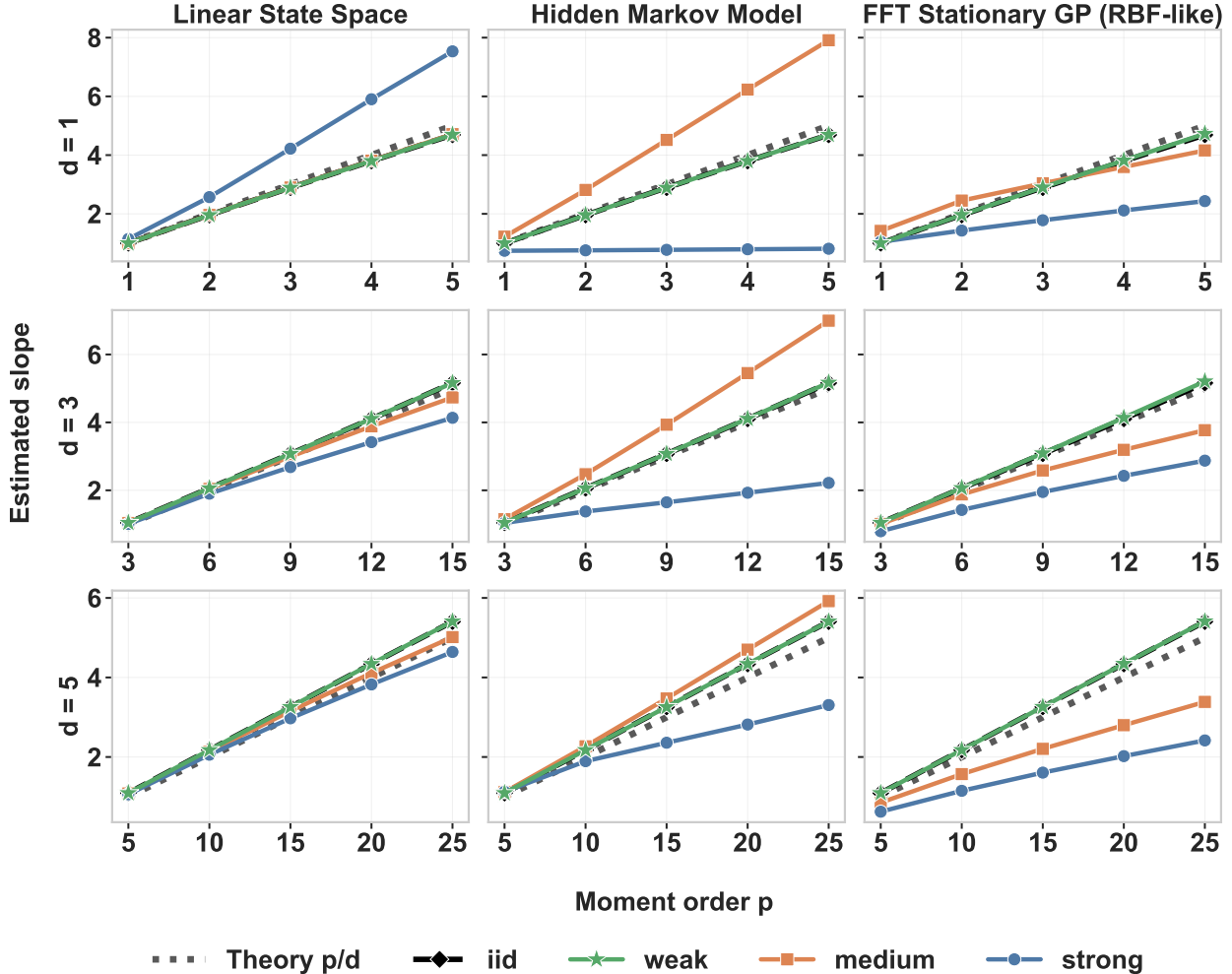


Figure 1: Slope summary for Experiment 1: rows correspond to  $d = 1, 3, 5$ , columns correspond to the three dependent model classes, and the shared legend compares the theoretical line  $p/d$ , the i.i.d. benchmark, and weak/medium/strong dependence.

Across the three data-generating processes (linear state-space, hidden Markov, and FFT Gaussian process), we impose weak/medium/strong dependence via model-specific persistence parameters. Figure 1 shows the expected pattern: weak dependence stays close to the i.i.d. baseline and the theoretical rate  $p/d$ , while medium and strong dependence diverge.

## 4.2 Entropy estimation

This experiment examines the intrinsic-dimension message of the nearest-neighbor theory in a representation-learning setting. We state our results in terms of a local intrinsic dimension  $s$ . A Kozachenko–Leonenko entropy estimate is built from the NN radii and the corresponding  $s$ -dimensional volume correction. Thus, if a learned representation preserves the local  $s$ -

dimensional geometry, the entropy estimator should converge to the entropy of the intrinsic process rather than behave as though the ambient dimension is a larger  $d$ . We consider the setup in which observations have ambient dimension  $d$ , but the true data-generating process has intrinsic dimension  $s$ .

The experiment generates an  $s$ -dimensional Gaussian AR(1) latent process, whose entropy is available in closed form as  $H_s = (s/2) \log(2\pi e)$ , and maps it into 20-dimensional observed data through a linear augmentation. Figure 2 reports the results for  $s \in \{1, 3, 5\}$  under three temporal-dependence regimes for the sample sequence: i.i.d. ( $\rho = 0$ ), weak AR(1) dependence ( $\rho = 0.3$ ), and strong AR(1) dependence ( $\rho = 0.6$ ), using the current run configuration with 1000 replications and number of NNs  $k = \max\{2, \lceil n^{0.1} \rceil\}$ . The oracle estimator on the latent  $s$ -dimensional data and the estimator based on the top  $s$  coordinates of a 5-component principal component analysis (PCA) representation both move toward the true entropy as  $n$  grows. Our reason for expecting the entropy estimator based on PCA to match the intrinsic-dimension behavior is that, in the implementation, the latent coordinates are independent across coordinates even though each coordinate follows the same AR(1) latent process. The 20-dimensional augmented observations are highly correlated in coordinates. PCA projects the observation to a low-dimensional representation, so the leading PCA coordinates are much closer to the intrinsic geometry and preserve the same weak-dependence structure. The comparison therefore supports the conclusion that PCA recovers the intrinsic entropy behavior and that weak dependence mainly changes constants rather than the qualitative convergence pattern; implementation details and numerical tables are left to the Appendix.

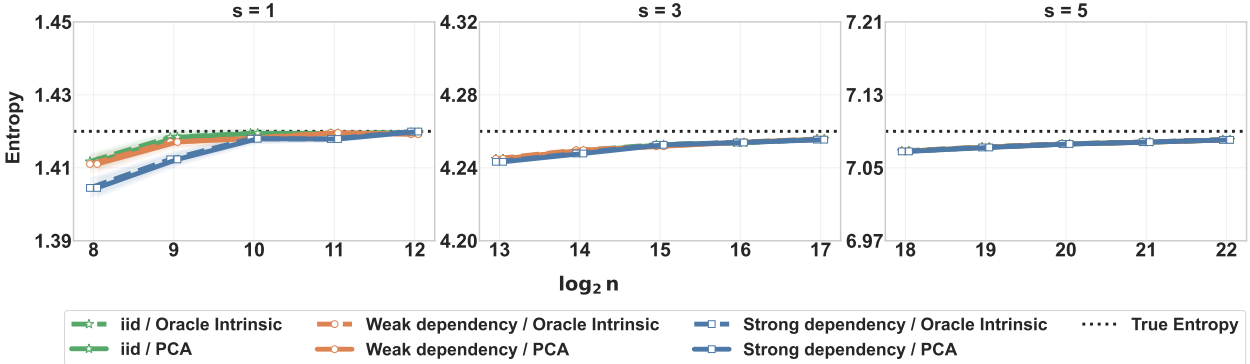


Figure 2: Experiment 2 entropy estimation. The dotted horizontal line is the true entropy. Colors encode the dependence level and markers distinguish the oracle intrinsic estimate from the PCA estimate.

### 4.3 Real-data evaluation

In this section, we complement the synthetic experiments with real-world time-series benchmarks. We compare two baselines: a raw  $k$ -nearest-neighbors (Raw- $k$ NN) method operating directly in standardized observation space, and a PCA  $k$ -nearest-neighbors (PCA- $k$ NN) method that first projects each input onto a lower-dimensional representation using PCA before applying nearest-neighbor prediction. We evaluate Raw- $k$ NN and PCA- $k$ NN on three real-data tasks: long-horizon forecasting, short-horizon forecasting, and classification. The datasets are from the Time Series Pile (Goswami et al., 2024), a large public time-series benchmark collection that includes the Informer long-horizon forecasting datasets (Zhou et al., 2021), the Monash Time Series Forecasting Archive (Godahewa et al., 2021), and the UCR Time Series Archive (Dau et al., 2019). We follow the benchmark setup and compare our results against MOMENT, a family of pre-trained time-series foundation models (Goswami et al., 2024). In both models, the input features are standardized before nearest-neighbor prediction. We tune the number of neighbors  $k \in \{1, 3, 5, 7, 9, 15, 21, 31\}$ , the neighbor weighting scheme (uniform/distance), and the distance metric (Manhattan/Euclidean). For PCA- $k$ NN, we additionally tune the embedding dimension over  $\{8, 16, 32, 48, 64\}$ .

Table 1 summarizes average performance across datasets for long-horizon forecasting, short-horizon forecasting, and classification. Figure 3 reports long-horizon forecasting mean squared error (MSE) separately for each dataset and forecast horizon. Figure 4 provides complementary views of short-horizon forecasting and classification: its left panel shows short-horizon forecasting symmetric mean absolute percentage error (sMAPE) under both the within-group and source-to-target transfer settings, while its right panel shows the distribution of classification accuracy with MOMENT summary statistics included as reference lines. Together, these results are supportive in two main ways. First, Raw- $k$ NN and PCA- $k$ NN remain informative across all three task families. In long-horizon forecasting, the two methods achieve average MSE 0.628 and 0.627, respectively, compared with 0.617 for MOMENT. In short-horizon forecasting, both methods produce nontrivial predictions in both the within-group and source-to-target transfer settings, although errors increase substantially in the transfer setting. In classification, both methods achieve mean accuracy 0.748, compared with 0.794 for MOMENT. These findings indicate that nearest-neighbor structure remains informative on real dependent data. Second, Raw- $k$ NN and PCA- $k$ NN achieve similar performance across tasks, consistent with adaptation to the intrinsic dimension of dependent data even under dependence. Their relative advantage varies across datasets, but neither method consistently dominates the other.

Although MOMENT generally outperforms the Raw- $k$ NN and PCA- $k$ NN baselines, this does not contradict the theory. Both nearest-neighbor methods remain effective on real dependent data, and PCA- $k$ NN performs comparably to Raw- $k$ NN even after reducing the input dimension. This shows that dimension reduction can preserve the local structure needed for neighborhood-based prediction.

Table 1: Comparison of Raw- $k$ NN, PCA- $k$ NN, and MOMENT on real-data tasks under a common benchmark setup. Performance is averaged over datasets within each task; MOMENT results are taken from [Goswami et al. \(2024\)](#).

Task	Metric	Raw- $k$ NN	PCA- $k$ NN	MOMENT
Long-horizon forecasting	MSE	0.628	0.627	0.617
Classification	Accuracy	0.748	0.748	0.794
Short-horizon forecasting (within-group)	sMAPE	16.199	16.488	–
Short-horizon forecasting (transfer)	sMAPE	27.210	27.369	14.525

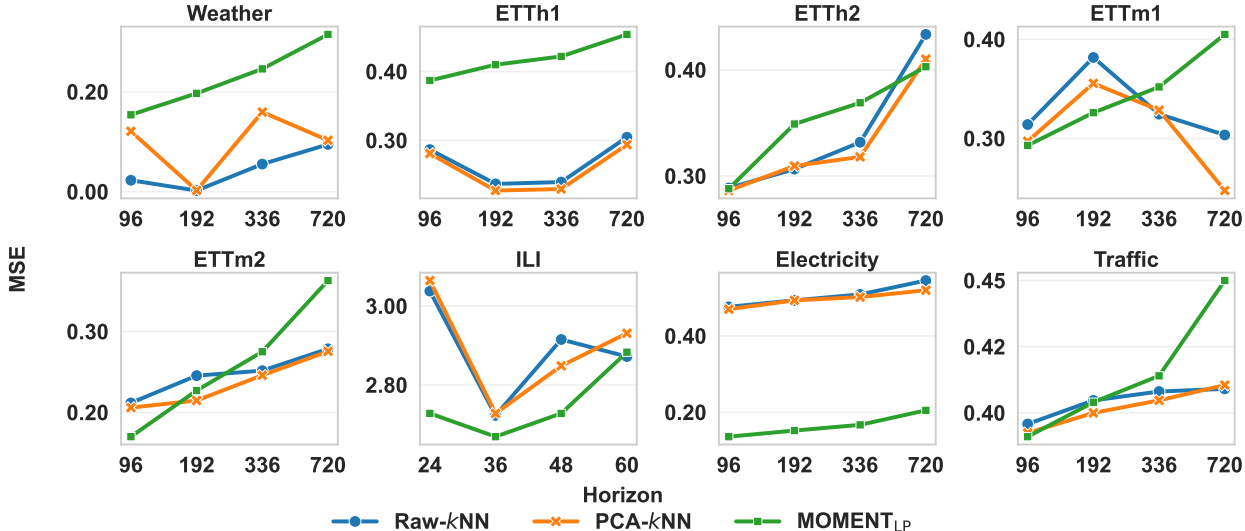


Figure 3: Comparison of long-horizon forecasting using test MSE across datasets and forecast horizons. It compares Raw- $k$ NN and PCA- $k$ NN with MOMENT across benchmark settings.

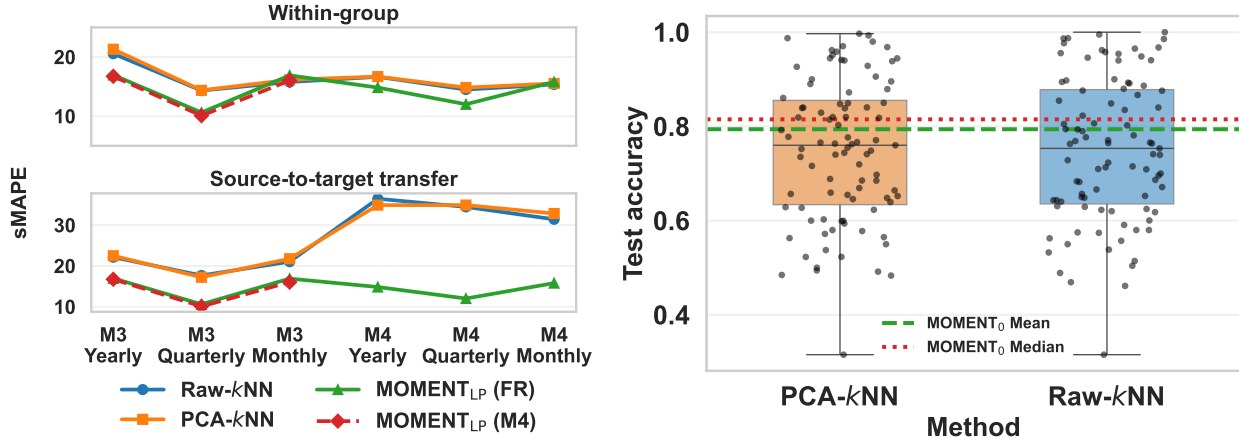


Figure 4: Comparisons on short-horizon forecasting and classification. The left panel compares forecasting under within-group and source-to-target transfer settings. The right panel shows classification accuracy across UCR datasets, with MOMENT summary statistics shown as reference lines.

## 5 Discussions

**Constants versus exponents.** One main message of the theory is that dependence and local geometry play qualitatively different roles. The local exponent  $s$  determines the fundamental scale  $(k/n)^{1/s}$ , whereas the dependence structure determines constants and concentration quality. This distinction is important both conceptually and empirically: it suggests that weak dependence should affect finite-sample behavior without changing the asymptotic behavior.

**On uniform convergence.** We study nearest-neighbor radii at a fixed query point  $x$ , both for almost sure convergence and for finite-sample tail and moment bounds. This pointwise analysis matches the local nature of nearest-neighbor methods and yields useful results for downstream learning methods at a given test point (Biau and Devroye, 2015). Extending the theory to uniform convergence over the support is interesting, especially for global guarantees on  $k$ -NN regression, classification, or graph construction (Biau and Devroye, 2015; Jiang, 2019). However, such a result would require additional assumptions and analysis: one would need the lower- and upper-mass conditions to hold uniformly over the support, together with uniform concentration for the dependent counting process indexed by balls, which is typical in empirical process theory under mixing conditions (Yu, 1994). Since our goal is to isolate the effect of dependence on nearest-neighbor radii, we leave the general uniform theory to future work. The pointwise results are also standard in nonparametric theory, where one first identifies the local behavior at a fixed query point and then generalizes to global sup-norm

under stronger regularity conditions (Györfi et al., 2002).

**Implications for learning methods.** More broadly, we provide a geometric control principle for a wide class of learning methods under dependent sampling. Since the  $k$ -NN radius determines the effective neighborhood size around a query point, our results imply that, under geometric mixing, dependent observations behave as if the relevant scale were still  $(k/n)^{1/s}$  up to constants and a dependence-induced concentration penalty. As a result, many heuristics on the methods from the i.i.d. setting continue to apply. In particular, whenever the performance of a method is driven by the size of adaptive neighborhoods—as in  $k$ -NN regression, local averaging, adaptive bandwidth selection, graph construction, or neighborhood-based manifold methods—our results can be used as an ingredient to transfer the performance to dependent data. From this perspective, we isolate a basic geometric quantity whose behavior under dependence can serve as a building block for future analyses of nonparametric and graph learning algorithms.

## Acknowledgments

We thank Fang Han for partially motivating this work and for helpful comments.

## References

- Abadie, A. and Imbens, G. W. (2006). Large sample properties of matching estimators for average treatment effects. *Econometrica*, 74(1):235–267.
- Abadie, A. and Imbens, G. W. (2011). Bias-corrected matching estimators for average treatment effects. *Journal of Business & Economic Statistics*, 29(1):1–11.
- Ansuini, A., Laio, A., Macke, J. H., and Zoccolan, D. (2019). Intrinsic dimension of data representations in deep neural networks. *Advances in Neural Information Processing Systems*, 32.
- Avdiukhin, D., Chatziafratis, V., Fischer, O., and Yaroslavtsev, G. (2024). Embedding dimension of contrastive learning and  $k$ -nearest neighbors. *Advances in Neural Information Processing Systems*, 37:41359–41393.
- Azadkia, M. and Chatterjee, S. (2021). A simple measure of conditional dependence. *The Annals of Statistics*, 49(6):3070–3102.
- Belkin, M. and Niyogi, P. (2003). Laplacian eigenmaps for dimensionality reduction and data representation. *Neural Computation*, 15(6):1373–1396.

- Biau, G. and Devroye, L. (2015). *Lectures on the nearest neighbor method*, volume 246. Springer.
- Bradley, R. C. (2005). Basic properties of strong mixing conditions. a survey and some open questions. *Probability Surveys*, 2:107–144.
- Cattaneo, M. D., Han, F., and Lin, Z. (2025). On rosenbaum’s rank-based matching estimator. *Biometrika*, 112(1):asae062.
- Chatterjee, S. (2021). A new coefficient of correlation. *Journal of the American Statistical Association*, 116(536):2009–2022.
- Chen, Q., Zhao, B., Wang, H., Li, M., Liu, C., Li, Z., Yang, M., and Wang, J. (2021). Spann: Highly-efficient billion-scale approximate nearest neighborhood search. *Advances in Neural Information Processing Systems*, 34:5199–5212.
- Cover, T. and Hart, P. (1967). Nearest neighbor pattern classification. *IEEE transactions on information theory*, 13(1):21–27.
- Dau, H. A., Bagnall, A., Kamgar, K., Yeh, C.-C. M., Zhu, Y., Gharghabi, S., Ratanamahatana, C. A., and Keogh, E. (2019). The ucr time series archive. *IEEE/CAA Journal of Automatica Sinica*, 6(6):1293–1305.
- Davydov, Y. A. (1968). Convergence of distributions generated by stationary stochastic processes. *Theory of Probability & Its Applications*, 13(4):691–696.
- Doukhan, P. (2012). *Mixing: Properties and Examples*, volume 85. Springer Science & Business Media.
- Fefferman, C., Mitter, S., and Narayanan, H. (2016). Testing the manifold hypothesis. *Journal of the American Mathematical Society*, 29(4):983–1049.
- Friedman, J. H. and Rafsky, L. C. (1979). Multivariate generalizations of the wald-wolfowitz and smirnov two-sample tests. *The Annals of Statistics*, 7(4):697–717.
- Godahewa, R., Bergmeir, C., Webb, G. I., Hyndman, R. J., and Montero-Manso, P. (2021). Monash time series forecasting archive. *arXiv preprint arXiv:2105.06643*.
- Gorishniy, Y., Rubachev, I., Kartashev, N., Shlenskii, D., Kotelnikov, A., and Babenko, A. (2023). Tabr: Tabular deep learning meets nearest neighbors in 2023. *arXiv preprint arXiv:2307.14338*.
- Goswami, M., Szafer, K., Choudhry, A., Cai, Y., Li, S., and Dubrawski, A. (2024). Moment: A family of open time-series foundation models. In *International Conference on Machine Learning*.

- Györfi, L., Kohler, M., Krzyżak, A., and Walk, H. (2002). *A distribution-free theory of nonparametric regression*. Springer.
- Han, F. (2021). On extensions of rank correlation coefficients to multivariate spaces. *Bernoulli News*, 28(2):7–11.
- Han, F. and Huang, Z. (2024). Azadkia–chatterjee’s correlation coefficient adapts to manifold data. *The Annals of Applied Probability*, 34(6):5172–5210.
- Henze, N. and Penrose, M. D. (1999). On the multivariate runs test. *The Annals of Statistics*, 27(1):290–298.
- Holst, M. and Irle, A. (2001). Nearest neighbor classification with dependent training sequences. *The Annals of Statistics*, 29(5):1424–1442.
- Jääsaari, E., Hyvönen, V., and Roos, T. (2024). Lorann: Low-rank matrix factorization for approximate nearest neighbor search. *Advances in Neural Information Processing Systems*, 37:102121–102153.
- Jiang, H. (2019). Non-asymptotic uniform rates of consistency for k-nn regression. In *Proceedings of the AAAI Conference on Artificial Intelligence*, volume 33, pages 3999–4006.
- Khandelwal, U., Fan, A., Jurafsky, D., Zettlemoyer, L., and Lewis, M. (2021). Nearest neighbor machine translation. In *International Conference on Learning Representations*.
- Kozachenko, L. and Leonenko, N. N. (1987). Sample estimate of the entropy of a random vector. *Problemy Peredachi Informatsii*, 23(2):9–16.
- Kpotufe, S. (2011). k-nn regression adapts to local intrinsic dimension. *Advances in Neural Information Processing Systems*, 24.
- Kraskov, A., Stögbauer, H., and Grassberger, P. (2004). Estimating mutual information. *Physical Review E—Statistical, Nonlinear, and Soft Matter Physics*, 69(6):066138.
- Kulkarni, S. R. and Posner, S. E. (1995). Rates of convergence of nearest neighbor estimation under arbitrary sampling. *IEEE Transactions on Information Theory*, 41(4):1028–1039.
- Liebscher, E. (1996). Strong convergence of sums of  $\alpha$ -mixing random variables with applications to density estimation. *Stochastic Processes and Their Applications*, 65(1):69–80.
- Lin, Z., Ding, P., and Han, F. (2023). Estimation based on nearest neighbor matching: from density ratio to average treatment effect. *Econometrica*, 91(6):2187–2217.

- Lin, Z. and Han, F. (2022). Limit theorems of chatterjee’s rank correlation. *arXiv preprint arXiv:2204.08031*.
- Lin, Z. and Han, F. (2023). On boosting the power of chatterjee’s rank correlation. *Biometrika*, 110(2):283–299.
- Lin, Z. and Han, F. (2024). On the failure of the bootstrap for chatterjee’s rank correlation. *Biometrika*, 111(3):1063–1070.
- Lin, Z. and Han, F. (2025). On regression-adjusted imputation estimators of average treatment effects. *Journal of Econometrics*, 251:106080.
- Loftsgaarden, D. O. and Quesenberry, C. P. (1965). A nonparametric estimate of a multivariate density function. *The Annals of Mathematical Statistics*, 36(3):1049–1051.
- Long, X., Peng, C., and Li, Y. (2025). Mnn: Mixed nearest-neighbors for self-supervised learning. *Pattern Recognition*, 158:110998.
- Merlevède, F., Peligrad, M., and Rio, E. (2009). Bernstein inequality and moderate deviations under strong mixing conditions. In *High dimensional probability V: the Luminy volume*, volume 5, pages 273–293. Institute of Mathematical Statistics.
- Mohri, M. and Rostamizadeh, A. (2010). Stability bounds for stationary  $\phi$ -mixing and  $\beta$ -mixing processes. *Journal of Machine Learning Research*, 11:661–686.
- Mokkadem, A. (1988). Mixing properties of arma processes. *Stochastic Processes and Their Applications*, 29(2):309–315.
- Nizan, O. and Tal, A. (2024). k-nnn: nearest neighbors of neighbors for anomaly detection. In *Proceedings of the IEEE/CVF Winter conference on applications of computer vision*, pages 1005–1014.
- Nobel, A. B. (1999). Limits to classification and regression estimation from ergodic processes. *The Annals of Statistics*, 27(1):262–273.
- Rio, E. (1995). The functional law of the iterated logarithm for stationary strongly mixing sequences. *The Annals of Probability*, 23(3):1188–1203.
- Shi, H., Drton, M., and Han, F. (2024). On azadkia–chatterjee’s conditional dependence coefficient. *Bernoulli*, 30(2):851–877.
- Stone, C. J. (1977). Consistent nonparametric regression. *The Annals of Statistics*, 5(4):595–620.

- Tu, S., Frostig, R., and Soltanolkotabi, M. (2024). Learning from many trajectories. *Journal of Machine Learning Research*, 25(216):1–109.
- Wang, M., Xu, X., Yue, Q., and Wang, Y. (2021). A comprehensive survey and experimental comparison of graph-based approximate nearest neighbor search. *arXiv preprint arXiv:2101.12631*.
- Wu, Y., Zhang, H., and Huang, H. (2022). Retrievalguard: Provably robust 1-nearest neighbor image retrieval. In *International Conference on Machine Learning*, pages 24266–24279. PMLR.
- Xu, B., Wang, Q., Mao, Z., Lyu, Y., She, Q., and Zhang, Y. (2023a).  $k$  nn prompting: Beyond-context learning with calibration-free nearest neighbor inference. *arXiv preprint arXiv:2303.13824*.
- Xu, F. F., Alon, U., and Neubig, G. (2023b). Why do nearest neighbor language models work? In *International Conference on Machine Learning*, pages 38325–38341. PMLR.
- Yang, M., Cai, Y., and Zheng, W. (2024). Cspg: crossing sparse proximity graphs for approximate nearest neighbor search. *Advances in Neural Information Processing Systems*, 37:103076–103100.
- Yu, B. (1994). Rates of convergence for empirical processes of stationary mixing sequences. *The Annals of Probability*, 22(1):94–116.
- Zhou, H., Zhang, S., Peng, J., Zhang, S., Li, J., Xiong, H., and Zhang, W. (2021). Informer: Beyond efficient transformer for long sequence time-series forecasting. In *Proceedings of the AAAI conference on artificial intelligence*, volume 35, pages 11106–11115.
- Zhu, X., Ghahramani, Z., and Lafferty, J. D. (2003). Semi-supervised learning using gaussian fields and harmonic functions. In *Proceedings of the 20th International conference on Machine learning (ICML-03)*, pages 912–919.

# A Proofs

We begin with a Bernstein-type inequality for  $\alpha$ -mixing sequences.

**Lemma 1** (Theorem 5 of [Rio \(1995\)](#); Theorem 2.1 of [Liebscher \(1996\)](#)). *Let  $[Z_i]_{i=1}^n$  be a centered sequence of random variables such that*

$$\mathbb{E}[Z_i] = 0 \quad \text{and} \quad |Z_i| \leq S(n) < \infty, \quad i \in \llbracket n \rrbracket.$$

*Then, for any  $n \geq 1$ , any  $m \in \llbracket n \rrbracket$ , and any  $\epsilon > 4mS(n)$ ,*

$$\mathbb{P}\left(\left|\sum_{i=1}^n Z_i\right| > \epsilon\right) \leq 4 \exp\left(-\frac{\epsilon^2}{64\frac{n}{m}\sigma_{n,m}^2 + \frac{8}{3}\epsilon m S(n)}\right) + 4\frac{n}{m}\alpha_m,$$

where

$$\sigma_{n,m}^2 := \sup_{0 \leq j \leq n-1} \mathbb{E}\left[\sum_{i=j+1}^{(j+m) \wedge n} Z_i\right]^2.$$

## A.1 Proof of Theorem 1

*Proof.* Fix  $x \in \mathbb{R}^d$ . Since  $\mathcal{X}_{(k)}^n(x) \in \text{supp}(\mu)$  almost surely and  $r_x = \inf\{\|y - x\| : y \in \text{supp}(\mu)\}$ , we have

$$\|\mathcal{X}_{(k)}^n(x) - x\| \geq r_x \quad \text{a.s. for every } n.$$

Thus, it remains to prove that

$$\limsup_{n \rightarrow \infty} \|\mathcal{X}_{(k)}^n(x) - x\| \leq r_x \quad \text{a.s.}$$

Fix  $\epsilon > 0$ , and define

$$p_x := \mu(B_{x, r_x + \epsilon}) = \mathbb{P}(\|X_{n,i} - x\| \leq r_x + \epsilon).$$

Since  $B_{x, r_x + \epsilon}$  intersects  $\text{supp}(\mu)$  by definition of  $r_x$ , we have  $p_x > 0$ .

We observe that the event  $\|\mathcal{X}_{(k)}^n(x) - x\| > r_x + \epsilon$  occurs if and only if fewer than  $k$  observations in the  $n$ -th row fall inside  $B_{x, r_x + \epsilon}$ . Then we have

$$\mathbb{P}(\|\mathcal{X}_{(k)}^n(x) - x\| > r_x + \epsilon) = \mathbb{P}\left(\sum_{i=1}^n \mathbf{1}\{\|X_{n,i} - x\| \leq r_x + \epsilon\} < k\right).$$

We set

$$Z_{n,i} := \mathbf{1}\{\|X_{n,i} - x\| \leq r_x + \epsilon\} - \mathbb{P}(\|X_{n,i} - x\| \leq r_x + \epsilon) = \mathbf{1}\{\|X_{n,i} - x\| \leq r_x + \epsilon\} - p_x.$$

Then  $\mathbb{E}[Z_{n,i}] = 0$  and  $|Z_{n,i}| \leq 1$ . Since  $Z_{n,i}$  is a measurable function of  $X_{n,i}$ , the sequence  $[Z_{n,i}]_{i=1}^n$  is again  $\alpha$ -mixing with the same mixing coefficients as  $[X_{n,i}]_{i=1}^n$ . Moreover, for any  $m \in \{1, \dots, n\}$  and any  $0 \leq j \leq n-1$ , the covariance inequality ([Davydov, 1968](#), Corollary

of Lemma 2.1) yields

$$\begin{aligned}
\mathbb{E} \left[ \sum_{i=j+1}^{(j+m)\wedge n} Z_{n,i} \right]^2 &= \text{Var} \left( \sum_{i=j+1}^{(j+m)\wedge n} Z_{n,i} \right) \\
&\leq \sum_{i=j+1}^{(j+m)\wedge n} \text{Var}(Z_{n,i}) + 2 \sum_{i=j+1}^{(j+m)\wedge n} \sum_{k>i} \text{Cov}(Z_{n,i}, Z_{n,k}) \\
&\leq m + 24 \sum_{i=j+1}^{(j+m)\wedge n} \sum_{k>i} \alpha_{k-i} \|Z_{n,i}\|_\infty \|Z_{n,k}\|_\infty \\
&\leq m + 24 \sum_{i=j+1}^{(j+m)\wedge n} \sum_{k>i} \alpha_{k-i} \\
&\leq m + 24m \sum_{\ell=1}^{\infty} \alpha_\ell.
\end{aligned}$$

Since  $\sum_{\ell=1}^{\infty} \alpha_\ell < \infty$ , we set  $M = 1 + 24 \sum_{\ell=1}^{\infty} \alpha_\ell < \infty$ , then

$$\sigma_{n,m}^2 := \sup_{0 \leq j \leq n-1} \mathbb{E} \left[ \sum_{i=j+1}^{(j+m)\wedge n} Z_{n,i} \right]^2 \leq Mm.$$

Since  $k/n \rightarrow 0$  and  $p_x > 0$ , for all sufficiently large  $n$ , we have  $k - np_x \leq -\frac{np_x}{2}$ . Then

$$\begin{aligned}
\mathbb{P}(\|\mathcal{X}_{(k)}^n(x) - x\| > r_x + \varepsilon) &= \mathbb{P}\left(\sum_{i=1}^n Z_{n,i} < k - np_x\right) \\
&\leq \mathbb{P}\left(\left|\sum_{i=1}^n Z_{n,i}\right| > np_x - k\right) \\
&\leq \mathbb{P}\left(\left|\sum_{i=1}^n Z_{n,i}\right| > \frac{np_x}{2}\right).
\end{aligned}$$

We now apply Lemma 1 with  $m_n = \lfloor \frac{3}{64} \frac{np_x}{\log n} \rfloor$ . Then  $m_n \rightarrow \infty$  and  $m_n/n \rightarrow 0$ . Therefore for all sufficiently large  $n$ , we have  $64M \leq \frac{4}{3} p_x m_n$  and  $\frac{np_x}{2} > 4m_n$ , and then the conditions of Lemma 1 are satisfied with  $S(n) = 1$  and  $\epsilon_n = np_x/2$ . Using  $\sigma_{n,m_n}^2 \leq Mm_n$ , we obtain

$$\begin{aligned}
\mathbb{P}\left(\left|\sum_{i=1}^n Z_{n,i}\right| > \frac{np_x}{2}\right) &\leq 4 \exp \left[ -\frac{(np_x/2)^2}{64(n/m_n)\sigma_{n,m_n}^2 + \frac{8}{3}(np_x/2)m_n} \right] + 4 \frac{n}{m_n} \alpha_{m_n} \\
&\leq 4 \exp \left[ -\frac{n^2 p_x^2 / 4}{64Mn + \frac{4}{3} np_x m_n} \right] + 4 \frac{n}{m_n} \alpha_{m_n} \\
&\leq 4 \exp \left[ -\frac{n^2 p_x^2 / 4}{\frac{8}{3} np_x m_n} \right] + 4 \frac{n}{m_n} \alpha_{m_n}
\end{aligned}$$

$$= 4 \exp\left(-\frac{3}{32} \frac{np_x}{m_n}\right) + 4 \frac{n}{m_n} \alpha_{m_n}.$$

By the choice of  $m_n$ , the exponential term is  $O(n^{-2})$ .

We now assume the mixing coefficients satisfy  $\alpha_m \lesssim m^{-(1+\gamma)}$  for some  $\gamma > 1$ . Then

$$\frac{n}{m_n} \alpha_{m_n} \lesssim \frac{n}{m_n^{2+\gamma}} \lesssim \frac{(\log n)^{2+\gamma}}{n^{1+\gamma}},$$

which is summable in  $n$ . Then

$$\sum_{n=1}^{\infty} \mathbb{P}(\|\mathcal{X}_{(k)}^n(x) - x\| > r_x + \varepsilon) < \infty.$$

By the Borel–Cantelli lemma,

$$\mathbb{P}(\|\mathcal{X}_{(k)}^n(x) - x\| > r_x + \varepsilon \text{ i.o.}) = 0.$$

That is, for every fixed  $\varepsilon > 0$ ,

$$\|\mathcal{X}_{(k)}^n(x) - x\| \leq r_x + \varepsilon \quad \text{eventually a.s.}$$

Let  $\varepsilon = 1/j$ ,  $j \in \mathbb{N}$ , and intersect the resulting probability-one events. Then we obtain

$$\limsup_{n \rightarrow \infty} \|\mathcal{X}_{(k)}^n(x) - x\| \leq r_x \quad \text{a.s.}$$

Together with the lower bound  $\|\mathcal{X}_{(k)}^n(x) - x\| \geq r_x$  a.s. for every  $n$ , we obtain

$$\|\mathcal{X}_{(k)}^n(x) - x\| \rightarrow r_x \quad \text{almost surely.}$$

This completes the proof. □

## A.2 Proof of Theorem 2

*Proof.* Fix  $r > 0$ , and define

$$Y_i(r) := \mathbf{1}\{\|X_{n,i} - x\| \leq r\}, \quad p_r := \mathbb{E}[Y_i(r)] = \mu(B(x, r)).$$

Let

$$N_n(x, r) := \sum_{i=1}^n Y_i(r).$$

By the definition of the  $k$ -nearest-neighbor radius,

$$R_{n,k}(x) > r \iff N_n(x, r) < k.$$

We now use a blocking argument. Partition the row into alternating kept and discarded blocks of length  $b_n$ . Set  $M_n = \lfloor \frac{n}{2b_n} \rfloor$ , and for  $u = 1, \dots, M_n$ , define the kept block

$$I_u := \{(2u - 2)b_n + 1, \dots, (2u - 1)b_n\}.$$

Let

$$W_u(r) := \sum_{i \in I_u} Y_i(r), \quad S_n^{\text{keep}}(r) := \sum_{u=1}^{M_n} W_u(r).$$

Since  $S_n^{\text{keep}}(r) \leq N_n(x, r)$ , we obtain

$$\mathbb{P}(R_{n,k}(x) > r) = \mathbb{P}(N_n(x, r) < k) \leq \mathbb{P}(S_n^{\text{keep}}(r) < k).$$

Consider the radius

$$r_j = 2^j r_*(n, k) = 2^j \left( \frac{8k}{c_- n} \right)^{1/s}, \quad j \geq 0,$$

and assume  $r_j \leq r_0$ . By Assumption 2,

$$p_{r_j} = \mu(B(x, r_j)) \geq c_- r_j^s = 8 \cdot 2^{js} \frac{k}{n}.$$

Since  $b_n/n \rightarrow 0$  and  $M_n b_n \geq n/4$  for all sufficiently large  $n$ ,

$$\mu_j = \mathbb{E}[S_n^{\text{keep}}(r_j)] = M_n b_n p_{r_j} \geq n p_{r_j} / 4 \geq 2^{js+1} k.$$

Therefore, on the event  $\{S_n^{\text{keep}}(r_j) < k\}$ , since  $\mu_j \geq 2k$ ,

$$\mu_j - S_n^{\text{keep}}(r_j) > \mu_j - k \geq \mu_j / 2.$$

Then

$$\{S_n^{\text{keep}}(r_j) < k\} \subseteq \left\{ \left| S_n^{\text{keep}}(r_j) - \mu_j \right| > \frac{\mu_j}{2} \right\}.$$

Therefore, if we define

$$Z_u := W_u(r_j) - \mathbb{E}[W_u(r_j)], \quad u = 1, \dots, M_n,$$

we have

$$\mathbb{P}(R_{n,k}(x) > r_j) \leq \mathbb{P}\left( \left| \sum_{u=1}^{M_n} Z_u \right| > \frac{\mu_j}{2} \right).$$

Next we apply Lemma 1 for the block sequence  $[Z_u]_{u=1}^{M_n}$ . Since each  $Z_u$  is measurable with respect to the coordinates in the kept block  $I_u$ , and successive kept blocks are separated by a discarded block of length  $b_n$ , the sequence  $[Z_u]_{u=1}^{M_n}$  is  $\alpha$ -mixing with coefficients

$$\bar{\alpha}_\ell := \sup_{u \geq 1} \sup_{A \in \sigma(Z_1, \dots, Z_u), B \in \sigma(Z_{u+\ell}, Z_{u+\ell+1}, \dots)} |\mathbb{P}(A \cap B) - \mathbb{P}(A)\mathbb{P}(B)| \leq \alpha_{\ell b_n}, \quad \ell \geq 1.$$

In particular,  $\bar{\alpha}_1 \leq \alpha_{b_n} \leq e^{-\gamma b_n} \leq n^{-8}$ , as long as  $b_n$  is chosen with a sufficiently large constant times  $\log n$ . Also,  $0 \leq W_u(r_j) \leq b_n$ , so  $|Z_u| = |W_u(r_j) - \mathbb{E}W_u(r_j)| \leq b_n$ . Thus the boundedness parameter in Lemma 1 is  $S(M_n) = b_n$ .

To bound the variance term  $\sigma_{M_n,1}^2$ , since  $W_u(r_j)$  is a sum of  $b_n$  Bernoulli indicators, we have  $W_u(r_j)^2 \leq b_n W_u(r_j)$ , and therefore

$$\text{Var}(Z_u) \leq \mathbb{E}[W_u(r_j)^2] \leq b_n \mathbb{E}[W_u(r_j)] = b_n^2 p_{r_j}.$$

Then for the block sequence with block parameter  $m = 1$ ,

$$\sigma_{M_n,1}^2 = \sup_{0 \leq v \leq M_n - 1} \mathbb{E}[Z_{v+1}^2] \leq b_n^2 p_{r_j}.$$

We now apply Lemma 1 to  $[Z_u]_{u=1}^{M_n}$  with  $m = 1$  and threshold  $\varepsilon = \mu_j/2 = M_n b_n p_{r_j}/2$ . Since  $\varepsilon \geq k \geq K_0 \log n$ , and  $b_n \asymp \log n$ , we may choose  $K_0$  sufficiently large so that  $\varepsilon > 4b_n$  for all sufficiently large  $n$ . Then by Lemma 1,

$$\begin{aligned} \mathbb{P}\left(\left|\sum_{u=1}^{M_n} Z_u\right| > \frac{\mu_j}{2}\right) &\leq 4 \exp\left(-\frac{(\mu_j/2)^2}{64M_n\sigma_{M_n,1}^2 + \frac{8}{3}(\mu_j/2)b_n}\right) + 4M_n\bar{\alpha}_1 \\ &\leq 4 \exp\left(-\frac{(\mu_j/2)^2}{64M_nb_n^2p_{r_j} + \frac{4}{3}\mu_jb_n}\right) + 4M_n\bar{\alpha}_1. \end{aligned}$$

Using  $\mu_j = M_n b_n p_{r_j}$ , we obtain  $\frac{4}{3}\mu_j b_n = \frac{4}{3}M_n b_n^2 p_{r_j}$ , so the denominator is bounded by

$$\left(64 + \frac{4}{3}\right) M_n b_n^2 p_{r_j} \leq 66 M_n b_n^2 p_{r_j},$$

and then

$$\frac{(\mu_j/2)^2}{64M_nb_n^2p_{r_j} + \frac{4}{3}\mu_jb_n} \geq c \frac{\mu_j^2}{M_nb_n^2p_{r_j}} = c \frac{(M_nb_np_{r_j})^2}{M_nb_n^2p_{r_j}} = cM_np_{r_j}.$$

Since  $M_n \geq n/(4b_n)$  for all large  $n$ ,

$$M_np_{r_j} \geq \frac{n}{4b_n} \cdot 8 \cdot 2^{j_s} \frac{k}{n} = 2 \cdot 2^{j_s} \frac{k}{b_n}.$$

Therefore, for some universal constant  $c_0 > 0$ ,

$$\mathbb{P}(R_{n,k}(x) > r_j) \leq 4 \exp\left(-c_0 2^{j_s} \frac{k}{b_n}\right) + 4M_n\bar{\alpha}_1.$$

Finally, using  $b_n \asymp \log n$ ,  $\bar{\alpha}_1 \leq n^{-8}$ , and  $M_n \leq n/(2b_n)$ , we obtain  $4M_n\bar{\alpha}_1 \leq Cn^{-7}$ , and then

$$\mathbb{P}(R_{n,k}(x) > r_j) \leq 4 \exp\left(-c_0 2^{j_s} \frac{k}{\log n}\right) + Cn^{-7},$$

after adjusting constants. This completes the proof.  $\square$

### A.3 Proof of Theorem 3

*Proof.* Let

$$r_* = \left(\frac{8k}{c_- n}\right)^{1/s}$$

and choose  $J_0$  maximal such that  $2^{J_0} r_* \leq r_0$ . Since the support of  $\mu$  has diameter at most  $D$ , we have  $R_{n,k}(x) \leq D$  almost surely.

We decompose the moment over

$$\{R_{n,k}(x) \leq r_*\}, \quad \{2^j r_* < R_{n,k}(x) \leq 2^{j+1} r_*\}, \quad 0 \leq j \leq J_0 - 1, \quad \{R_{n,k}(x) > 2^{J_0} r_*\},$$

and we obtain

$$\mathbb{E}[R_{n,k}(x)^p] \leq r_*^p + \sum_{j=0}^{J_0-1} (2^{j+1} r_*)^p \mathbb{P}(R_{n,k}(x) > 2^j r_*) + D^p \mathbb{P}(R_{n,k}(x) > 2^{J_0} r_*).$$

We now apply Theorem 2. For every  $0 \leq j \leq J_0$ ,

$$\mathbb{P}(R_{n,k}(x) > 2^j r_*) \leq 4 \exp\left(-c_0 2^{js} \frac{k}{\log n}\right) + Cn^{-7},$$

and then

$$\mathbb{E}[R_{n,k}(x)^p] \leq r_*^p + Cr_*^p \sum_{j=0}^{J_0-1} 2^{jp} \exp\left(-c_0 2^{js} \frac{k}{\log n}\right) + Cr_*^p n^{-7} \sum_{j=0}^{J_0-1} 2^{jp} + CD^p n^{-7}.$$

We now bound the three terms on the right-hand side. For the first term, since  $k \geq K_0 \log n$ , the quantity  $k/\log n$  is bounded below by a positive constant. Therefore

$$\sum_{j=0}^{J_0-1} 2^{jp} \exp\left(-c_0 2^{js} \frac{k}{\log n}\right) \leq \sum_{j \geq 0} 2^{jp} e^{-c_1 2^{js}} < \infty$$

for some constant  $c_1 > 0$ . For the second term, since  $2^{J_0} r_* \leq r_0 < 2^{J_0+1} r_*$ , we have  $2^{J_0} \asymp r_*^{-1}$ , where the constants depend only on  $r_0$ . Then

$$r_*^p \sum_{j=0}^{J_0-1} 2^{jp} \leq Cr_*^p 2^{J_0 p} \leq C,$$

and then

$$Cr_*^p n^{-7} \sum_{j=0}^{J_0-1} 2^{jp} \leq Cn^{-7},$$

which is negligible. The third term  $CD^p n^{-7}$  is negligible as well. Combining the above estimates yields

$$\mathbb{E}[R_{n,k}(x)^p] \leq Cr_*^p + Cn^{-7} \leq Cr_*^p.$$

Since

$$r_*^p = \left(\frac{8k}{c_- n}\right)^{p/s} \asymp \left(\frac{k}{n}\right)^{p/s},$$

we obtain

$$\mathbb{E}[R_{n,k}(x)^p] \leq C \left(\frac{k}{n}\right)^{p/s}.$$

This completes the proof. □

## A.4 Proof of Theorem 4

*Proof.* Let

$$r^- = \left( \frac{k}{2c_+n} \right)^{1/s}.$$

By Assumption 3,

$$\mu(B(x, r^-)) \leq c_+(r^-)^s = \frac{k}{2n}.$$

Therefore,

$$\mathbb{E}[N_n(x, r^-)] = n \mu(B(x, r^-)) \leq k/2,$$

where,

$$N_n(x, r) = \sum_{i=1}^n \mathbf{1}\{\|X_{n,i} - x\| \leq r\}.$$

By Markov's inequality,

$$\mathbb{P}(N_n(x, r^-) \geq k) \leq \frac{\mathbb{E}[N_n(x, r^-)]}{k} \leq \frac{1}{2},$$

and

$$R_{n,k}(x) > r^- \iff N_n(x, r^-) < k,$$

we have

$$\mathbb{P}(R_{n,k}(x) > r^-) \geq \frac{1}{2}.$$

On the event  $\{R_{n,k}(x) > r^-\}$ , we have  $R_{n,k}(x)^p \geq (r^-)^p$ , and then

$$\mathbb{E}[R_{n,k}(x)^p] \geq (r^-)^p \mathbb{P}(R_{n,k}(x) > r^-) \geq \frac{1}{2} (r^-)^p.$$

By the definition of  $r^-$ , we obtain

$$\mathbb{E}[R_{n,k}(x)^p] \geq \frac{1}{2} \left( \frac{k}{2c_+n} \right)^{p/s}.$$

This completes the proof. □

## A.5 Proof of Theorem 5

*Proof.* The conclusion follows directly by combining the upper and lower bounds established in Theorems 3 and 4. □

## B Experiments

We provide additional details on the implementation of the experiments.

Table 2: Dependence-strength settings for the three dependent DGPs in experiment 1. Weak settings are near i.i.d., while medium and strong settings increase dependence contrast.

Model	Tuning parameter	Weak	Medium	Strong
Linear Gaussian state-space (factor AR(1))	AR coefficient $\rho$	0.02	0.60	0.98
Hidden Markov model (2-state)	Stay probability $p_{\text{stay}}$	0.70	0.99	0.9995
Gaussian process (FFT, RBF)	Lengthscale $\ell$	1	50	200

## B.1 Experiment 1 (Section 4.1) implementation details

**Setup.** Experiment 1 uses interior query aggregation. For each MC replication, we sample

$$X_{\text{eval}} \sim \text{Unif}([0.01, 0.99]^d), \quad |X_{\text{eval}}| = 1000,$$

The number of NNs is chosen as  $k = \lfloor n^\beta \rfloor$  with  $\beta$  on a 20-point grid in  $[0.1, 0.9]$  for slope fitting. We also impose a cap for  $\frac{k}{n} \leq 0.01$ .

**Data generating processes.** The i.i.d. uniform data is used as the baseline in every panel. The dependent data is generated by the following processes, with three strength levels, as shown in Table 2.

- **Linear Gaussian state-space (LSS).** A shared latent AR(1) factor is generated as

$$f_t = \rho f_{t-1} + \sqrt{1 - \rho^2} \eta_t, \quad \eta_t \sim \mathcal{N}(0, 1).$$

Then each coordinate is

$$z_{t,j} = a f_t + \sqrt{1 - a^2} \varepsilon_{t,j}, \quad \varepsilon_{t,j} \sim \mathcal{N}(0, 1),$$

with dimension-damped shared loading

$$a = \frac{s\sqrt{|\rho|}}{d^\gamma}, \quad s = 0.9, \gamma = 0.3.$$

(Implementation clips  $a \in [0, 0.999]$  and uses burn-in 400.)

- **Hidden Markov model (HMM).** Each coordinate  $j$  has its own two-state chain  $S_{t,j} \in \{0, 1\}$  with

$$\text{P}(S_{t,j} = S_{t-1,j}) = p_{\text{stay}}.$$

Conditional emissions are

$$Z_{t,j} \mid S_{t,j} \sim \mathcal{N}((2S_{t,j} - 1)\mu_{\text{eff}}, \sigma^2),$$

where  $\mu = 1.75$ ,  $\sigma = 0.70$ , and

$$\mu_{\text{eff}} = \mu |2p_{\text{stay}} - 1|^6.$$

(This keeps weak settings close to i.i.d. after marginal transformation while separating medium/strong regimes; burn-in 400.)

- **Gaussian process (FFT, RBF).** For each coordinate, a stationary Gaussian sequence is generated with lag covariance

$$k(h) = \exp\left(-\frac{h^2}{2\ell^2}\right), \quad \ell \in \{1, 50, 200\},$$

using circulant embedding and FFT spectral filtering ( $O(n \log n)$ ), then truncating to length  $n$ .

- **Transformation.** All  $d$  coordinates are transformed to have approximately  $\text{Unif}[0, 1]$  marginal distributions while retaining dependence:

$$U_{t,j} = \Phi(Z_{t,j}) \quad (\text{LSS/GP}),$$

and, for HMM, via the stationary two-component mixture CDF

$$F_{\text{mix}}(z) = \frac{1}{2}\Phi\left(\frac{z + \mu_{\text{eff}}}{\sigma}\right) + \frac{1}{2}\Phi\left(\frac{z - \mu_{\text{eff}}}{\sigma}\right).$$

## B.2 Experiment 2 (Section 4.2) implementation details

**Data-generating process.** For each intrinsic dimension  $s$ , we generate independent stationary Gaussian AR(1) latent processes across coordinates:

$$Z_t = \rho Z_{t-1} + \sqrt{1 - \rho^2} \varepsilon_t, \quad \varepsilon_t \sim \mathcal{N}(0, I_s).$$

The temporal dependence levels are  $\rho = 0$  for the i.i.d. benchmark,  $\rho = 0.3$  for weak AR(1) dependence, and  $\rho = 0.6$  for strong AR(1) dependence. The latent coordinates are independent across dimensions, while each coordinate follows the same AR(1) dependence over time. The latent vector is embedded into a 5-dimensional signal representation and then mapped into 20 observed coordinates by a fixed orthonormal  $20 \times 5$  linear map, which induces a low-rank cross-coordinate dependence structure in the ambient observations. The PCA estimator fits a 5-component PCA representation to the observed data and then estimates entropy using the top  $s$  PCA coordinates, which, in this linear Gaussian setting, recover an orthogonal low-dimensional representation up to rotation.

**Estimators and simulation grid.** All reported curves use the Kozachenko–Leonenko  $k$ -NN entropy estimator with Euclidean distance. The oracle intrinsic estimate is computed on the true latent  $s$ -dimensional sample, and the PCA estimate is computed on the top  $s$  PCA coordinates. The current implementation uses 1000 Monte Carlo replications with global random seed 20260504, burn-in 2000, and neighbor schedule  $k = \max\{2, \lceil n^{0.1} \rceil\}$ .

## B.3 Experiment 3 (Section 4.3) implementation details

We follow the real-data benchmark setup of [Goswami et al. \(2024\)](#) for long-horizon forecasting, short-horizon forecasting, and classification, using the same task definitions, evaluation

metrics, and preprocessing procedures. In addition to the source-to-target short-horizon setting considered in [Goswami et al. \(2024\)](#), we also report a within-group short-horizon evaluation. The setup for each task is as follows.

- **Long-horizon forecasting.** We use 9 datasets from the Informer long-horizon forecasting benchmark: ETTm1, ETTm2, ETTh1, ETTh2, Electricity, Traffic, Weather, Exchange, and ILI. The evaluation metrics are MSE and mean absolute error (MAE). We use a look-back window length of 512 and a horizontal 60/10/30 train/validation/test split, with forecast horizons  $\{24, 36, 48, 60\}$  for ILI and  $\{96, 192, 336, 720\}$  otherwise. Hyperparameters are selected by 5-fold time-series cross-validation when the training set contains at least 20 windows, and by validation-holdout tuning otherwise.
- **Short-horizon forecasting.** We use 6 benchmark groups from the Monash time series forecasting archive: M4-Yearly, M4-Quarterly, M4-Monthly, M3-Yearly, M3-Quarterly, and M3-Monthly. The evaluation metric is sMAPE, and the input length is 512. In the source-to-target transfer setting, hyperparameters are selected on a source group and evaluated directly on a different target group with the same frequency. We also report a within-group short-horizon evaluation, which is not included in the original MOMENT benchmark. In this setting, each dataset group is randomly split into a 70% source portion and a 30% target portion; hyperparameters are selected by 5-fold cross-validation on the source portion, and evaluation is performed on the target portion from the same group.
- **Classification.** We use 91 datasets from the UCR classification archive. The evaluation metric is accuracy. Inputs are represented as length-512 time series, and we use the official train/test splits provided by the UCR archive. Hyperparameters are selected using only the official training split, via stratified cross-validation when feasible, and final performance is evaluated on the official test split.

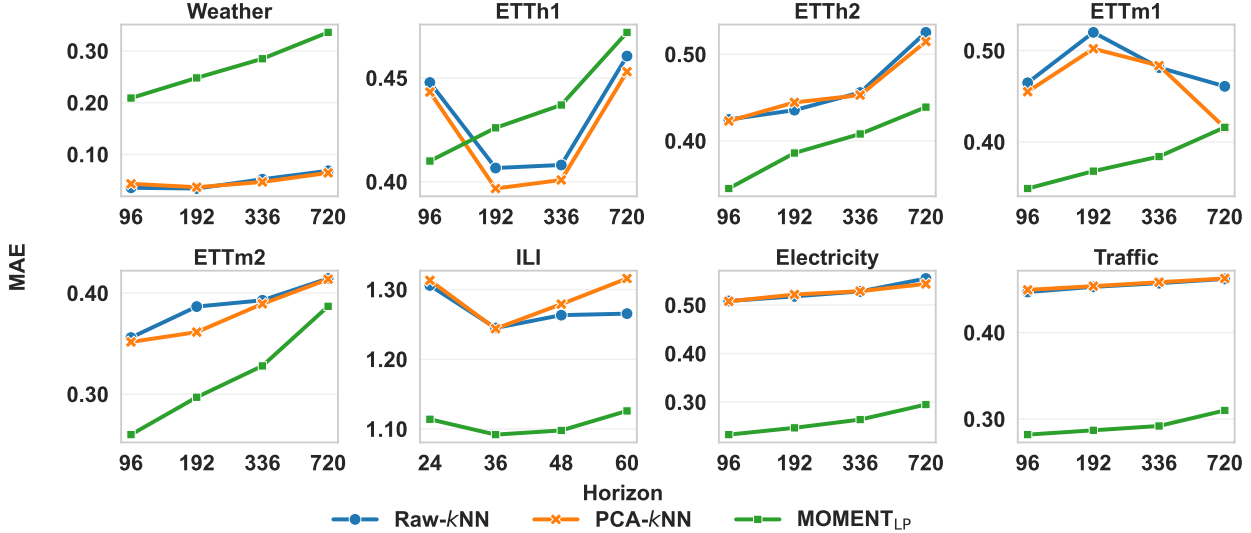


Figure 5: Comparison of long-horizon forecasting using test MAE across datasets and forecast horizons. It compares Raw- $k$ NN and PCA- $k$ NN with MOMENT across benchmark settings.

## B.4 Dataset availability

We use two types of datasets in this paper: synthetic datasets and real-world time-series benchmark datasets. The synthetic datasets in Experiments 4.1 and 4.2 are generated from the data-generating processes described in Appendices B.1 and B.2, respectively, using the global random seed 20260504. The real-world datasets in Experiment 4.3 are taken from the Time Series PILE (Goswami et al., 2024), which includes datasets from the Informer long-horizon forecasting benchmark, the Monash time series forecasting archive, and the UCR classification archive. These benchmark datasets are publicly available from their original sources.

## B.5 Code availability

Code for synthetic data generation, preprocessing, hyperparameter tuning, evaluation, and figure reproduction will be made publicly available upon publication. Experiments 4.1 and 4.2 were run entirely on CPU on a cluster node with two AMD EPYC 9754 128-Core Processors, comprising 256 physical cores and 256 hardware threads. Reproducing these two experiments takes approximately 5 hours. Experiment 4.3 was run entirely on CPU on a Linux workstation with an AMD EPYC 9554 64-Core Processor, comprising 64 physical cores and 128 hardware threads, and takes approximately 4 hours to reproduce. No GPU acceleration was used.

Table 3: Long-horizon forecasting results. We report test MSE and MAE for Raw- $k$ NN, PCA- $k$ NN, and MOMENT; MOMENT results are taken from Table 2 of [Goswami et al. \(2024\)](#).

Setting		Raw- $k$ NN		PCA- $k$ NN		MOMENT <sub>LP</sub>	
Dataset	Horizon	MSE	MAE	MSE	MAE	MSE	MAE
Weather	96	0.023	0.036	0.121	0.043	0.154	0.209
	192	0.002	0.034	0.003	0.037	0.197	0.248
	336	0.055	0.052	0.160	0.047	0.246	0.285
	720	0.095	0.068	0.103	0.064	0.315	0.336
ETTh1	96	0.287	0.448	0.281	0.443	0.387	0.410
	192	0.237	0.407	0.227	0.397	0.410	0.426
	336	0.239	0.408	0.229	0.401	0.422	0.437
	720	0.305	0.461	0.294	0.453	0.454	0.472
ETTh2	96	0.289	0.425	0.286	0.423	0.288	0.345
	192	0.306	0.436	0.309	0.444	0.349	0.386
	336	0.332	0.456	0.318	0.453	0.369	0.408
	720	0.433	0.525	0.410	0.515	0.403	0.439
ETTh1	96	0.314	0.465	0.297	0.455	0.293	0.349
	192	0.382	0.520	0.356	0.502	0.326	0.368
	336	0.325	0.481	0.328	0.484	0.352	0.384
	720	0.304	0.461	0.247	0.416	0.405	0.416
ETTh2	96	0.212	0.356	0.206	0.352	0.170	0.260
	192	0.245	0.387	0.215	0.361	0.227	0.297
	336	0.252	0.393	0.246	0.389	0.275	0.328
	720	0.279	0.415	0.275	0.414	0.363	0.387
ILI	24	3.038	1.306	3.065	1.313	2.728	1.114
	36	2.723	1.245	2.728	1.244	2.669	1.092
	48	2.915	1.263	2.848	1.279	2.728	1.098
	60	2.872	1.265	2.931	1.316	2.883	1.126
ECL	96	0.476	0.508	0.470	0.508	0.136	0.233
	192	0.493	0.518	0.493	0.522	0.152	0.247
	336	0.509	0.528	0.502	0.529	0.167	0.264
	720	0.545	0.555	0.520	0.544	0.205	0.295
Traffic	96	0.396	0.447	0.392	0.449	0.391	0.282
	192	0.405	0.453	0.400	0.454	0.404	0.287
	336	0.408	0.457	0.405	0.458	0.414	0.292
	720	0.409	0.462	0.410	0.463	0.450	0.310

Table 4: Classification accuracy across 91 UCR datasets. We report summary statistics for Raw- $k$ NN, PCA- $k$ NN, and MOMENT; MOMENT results are taken from Table 4 of [Goswami et al. \(2024\)](#).

Statistic	Raw- $k$ NN	PCA- $k$ NN	MOMENT <sub>0</sub>
Mean	0.748	0.748	0.794
Median	0.753	0.760	0.815
Std.	0.153	0.151	0.147

Table 5: Short-horizon forecasting results measured using sMAPE. We compare Raw- $k$ NN and PCA- $k$ NN transfer results with MOMENT results from Table 3 of [Goswami et al. \(2024\)](#) under the same source-to-target evaluation setting.

Setting		Raw- $k$ NN	PCA- $k$ NN	MOMENT <sub>LP</sub>	
Dataset	Frequency			M4	FR
M3	Yearly	22.14	22.50	16.74	16.97
	Quarterly	17.67	17.24	10.09	10.62
	Monthly	21.05	21.77	16.04	16.90
M4	Yearly	36.48	34.91	–	14.84
	Quarterly	34.48	34.93	–	12.02
	Monthly	31.44	32.86	–	15.80

Table 6: Short-horizon forecasting results measured using sMAPE under the within-group evaluation setting. We compare Raw- $k$ NN and PCA- $k$ NN with MOMENT results from Table 3 of [Goswami et al. \(2024\)](#).

Target series		Raw- $k$ NN	PCA- $k$ NN	MOMENT <sub>LP</sub>	
Dataset	Frequency			M4	FR
M3	Yearly	20.56	21.32	16.74	16.97
	Quarterly	14.33	14.38	10.09	10.62
	Monthly	15.78	16.17	16.04	16.90
M4	Yearly	16.65	16.69	–	14.84
	Quarterly	14.51	14.84	–	12.02
	Monthly	15.37	15.53	–	15.80